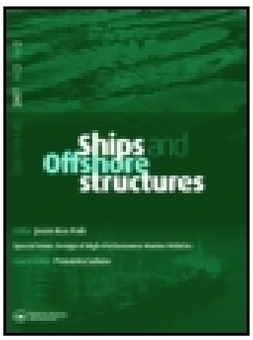

Taylor & Francis
Taylor & Francis Group

Ships and Offshore Structures

ISSN: 1744-5302 (Print) 1754-212X (Online) Journal homepage: https://www.tandfonline.com/loi/tsos20

Numerical testing and verification of a marine propeller operating in a uniform flow field

Howan Kim & Zhi Quan Leong

To cite this article: Howan Kim & Zhi Quan Leong (2020): Numerical testing and verification of a marine propeller operating in a uniform flow field, Ships and Offshore Structures

To link to this article: https://doi.org/10.1080/17445302.2019.1710917

Published online: 06 Jan 2020.

SHIPS AND OFFSHORE STRUCTURES
https://doi.org/10.1080/17445302.2019.1710917

Taylor & Francis
Taylor & Francis Group

Numerical testing and verification of a marine propeller operating in a uniform flow field

Howan Kim and Zhi Quan Leong

National Centre for Maritime Engineering and Hydrodynamics, Australian Maritime College, University of Tasmania, Newnham, Australia

ABSTRACT

This paper examines the methodology for the Reynolds Averaged Navier-Stokes (RANS) based Computational Fluid Dynamics (CFD) prediction of the flow around a propeller operating in a uniform flow. The work investigates the influence of grid and physics setup on the prediction of propeller propulsion properties (i.e. thrust (*Kt*) and torque (*Kq*) coefficients). The investigation includes the selection of the turbulence model, near wall gridding and state condition to achieve predictions comparable to experimental measurements. The prediction was validated against the experimental data from the open water propeller test conducted at the Australian Maritime College Cavitation Tunnel (AMCCT). The results show the CFD predictions were in good agreement with the experimental measurements (i.e. less than 5% at up to $J = 1.1$ and 10% at up to $J = 1.19$ for *Kt* and *Kq*). This confirms the presented methodology can be adopted to provide high fidelity prediction for the hydrodynamic characteristics of the propeller.

ARTICLE HISTORY
Received 1 March 2017
Accepted 28 December 2019

KEYWORDS
CFD; RANS; marine propeller; near wall gridding; turbulence model

1. Introduction

The investigation of the hydrodynamic performance of a propeller is imperative for a marine vehicle operating efficiently at a desired speed. An efficient propeller should provide maximum thrust and minimum torque for the optimum propeller rotation speed. These characteristics can be examined via propeller hydrodynamic performance curves representing thrust coefficient, torque coefficient, and efficiency as a function of advance speed ratio. The performance curves are typically obtained through an Open Water Test (OWT) via experimental testing. However, with the ongoing development of Computational Fluid Dynamics (CFD) technology and computing resource, the numerical simulations using CFD is increasingly used to complement the experimental testing (Kim et al. 2018). The CFD simulations can be performed based on Reynolds Averaged Navier-Stokes (RANS) or Large Eddy Simulations (LES). While the LES computation is capable of capturing the location and dynamic behaviour of the vortical structure around the propeller, the LES requires very fine near-wall grid resolution to accurately calculate the skin friction on the surface (Lu et al. 2012; Norrison et al. 2016). This might lead excessive grid counts resulting in great computational time and resource. However, the RANS can solve the simulation with comparatively less grid resolution, thus increasing the computational efficiency in time and resource. The major challenge for the RANS simulations is that the results greatly vary with the grid and numerical model settings (Kim 2018).

The present study examines the influence of the turbulence model using five different omega-based turbulence models with various near wall grids strategies involving y^+ value and inflation layer thickness. Other factor that influences the prediction such as state conditions (i.e. steady-state and transient) is also investigated. The methodology was applied to the computations of the hydrodynamic characteristics of a 5-blade submarine propeller operating in various inflow velocities. The predictions were validated against the experimental data obtained from the open water test conducted at the Australian Maritime College Cavitation Tunnel (AMCCT). From this study, the authors anticipate the developed methodology to be used for propeller modelling in a free-running manoeuvring simulation for a submarine.

2. Literature review

Over the past years, many researchers have reported the RANS based prediction method for the examination of hydrodynamic performance of a propeller operating in open water condition.

Rhee and Joshi (2005) proposed a hybrid grid generation strategy for RANS based computation of the hydrodynamic characteristics of a marine propeller at various inflow velocities. The prismatic grid was used on the near surface by prescribing 6 layers with y^+ ranging from 2 to 300. While the predictions for *Kt* matched well with the experimental data, *Kq* was over-predicted across the advance speed ratios (J) within the maximum of around 11% difference.

Lu et al. (2012) performed RANS computations for the open water propeller, having the diameter of 0.254 m with a pitch to diameter ratio (P/D) of 1.447. The test was conducted at the inflow velocity of 4.2 m/s and the rotational speed of 17.7rev/s, giving an advance speed ratio (J) of 0.934. The propeller geometry and test case were similar to the present simulation case (see Sections 3.1 and 3.2). The computational grid was comprised of tetrahedrals with prism layer of hexahedrals around

CONTACT Howan Kim Howan.Kim@utas.edu.au; Zhi Quan Leong Zhi.Leong@utas.edu.au

the propeller with the near wall grid resolution by $y^+ = 70–100$ of the major part of the blades. The CFD results showed that both the *Kt* and *Kq* were underpredicted by 9.2% and 2.4% compared to experimental data.

Morgut and Nobile (2012) studied the influence of grid type (i.e. hybrid-unstructured and hexa-structured grids) and turbulence model using Baseline Reynolds Stress Model (BSLRSM) and Shear Stress Transport (SST). The study indicated that the both grid types can provide similar levels of accuracy of the global field quantities unless detailed investigations of the flow field are needed, and the BSLRSM provided only slightly better predictions than the SST.

Peng et al. (2013) performed a numerical simulation of the open water marine propeller (i.e. DTMB 5168) using different grid resolutions and two different grid distributions with y^+ value set to 7.5. The effect of the grid resolution and distribution on the thrust and torque was found minimal. Also, the study found that the eddy viscosity turbulence models are performed slightly better to the Reynolds stress models, although the difference in the propeller performance prediction is insignificant. The study highlighted that the structured grid generation for the propeller is challenging due to the difficulty in maintaining small first grid spacings and smoothed grids orthogonal to the propeller blade surface. Thus, further work on improving grid quality near the surface was suggested.

Guilmineau et al. (2014) used *k-w* SST and EARSM to predict the open water characteristics of the propeller model. The grid was generated using only unstructured hexahedrons wiht 21.4 million cells. The average wall normal resolution on the blades was set as y^+ of 0.6. The study found that The k-*w* SST and EARSM showed very similar prediction for *Kt* and *Kq*.

Yao (2015) conducted a numerical study on investigating on hydrodynamic characteristics of a marine propeller. The RANS based computations were performed using *k-w* SST model without wall function. The tetra hedron grid was adopted with three triangular prism layer. The spacing of the first grid layer from the propeller surface was specified to 0.1 mm to prescribe a y^+ of appropriately 1.

Wang et al. (2017) used 8 layers of prismatic grids on the surface of blades and hub with the thickness of the first grid layer at 0.2 mm, corresponding to y^+ of about 60. The predition of *Kt* and *Kq* from Yao (2015) and Wang et al. (2017) showed a good correlation to experimental data, but the near wall gridding methodology for the selection of wall thickness and number of layers was missing.

The review of the literature revealed that the accuracy of the RANS based prediction of the propulsion properties is susceptible to the grid strategy and physics setup. However, the past work presented limited discussions on the influence of the turbulence model associated with near wall gridding methodology and state condition (i.e. steady-state and transient conditions) on the prediction. Thus, the present research was conducted to fill the gap in the discussion on RANS based simulation modelling methodology for an open water propeller.

3. Methodology

3.1. Propeller model

The present study utilised a 5-blade submarine propeller designed by the Defence Science and Technology (DST) group (Norrison et al. 2016) (see Figure 1). The propeller has a diametre (D) of 0.25 m, Hub diametre ratio (H/D) of 0.20 and Chord at 0.7 radius ($C_{0.7R}$) of 0.697×10^{-1}.

3.2. Test case

Table 1 outlines the open water test cases involving various inflow velocities (V) at a rotation rate (n) of 15rev/s. The advance speed ratio (J) was calculated based on $J = V/(nD)$.

3.3. CFD simulation setup

The numerical simulations were computed based on RANS equations using the commercial CFD software, ANSYS CFX v16. The numerical tank size was prescribed the same as the size of the experimental basin at AMCCT (see Figure 2). It is noted that the blockage correction was made in the experimental data to avoid the interference due to the confinement of the test section walls. This enables the experimental data

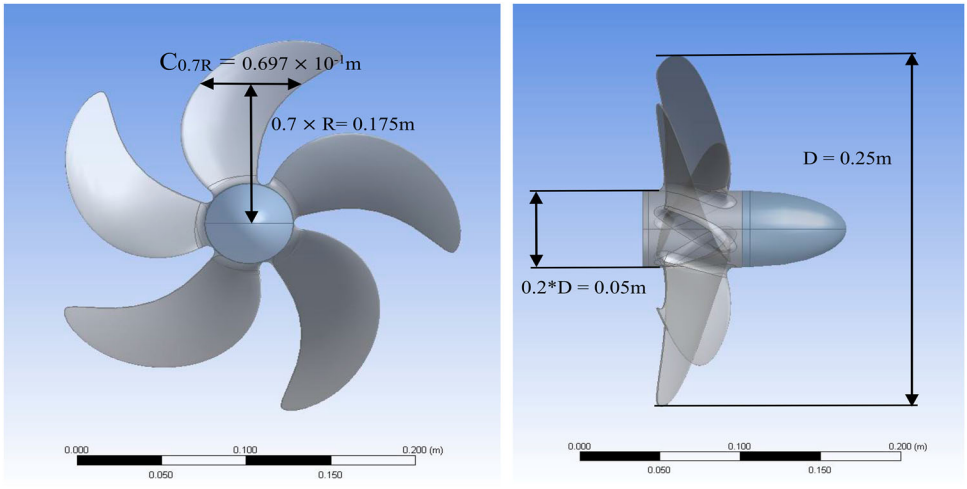

Figure 1. DST 5-blade propeller having a diametre (D) of 0.25 m, Hub diametre ratio (H/D) of 0.20, chord at 0.7R ($C_{0.7R}$) of 0.697×10^{-1} m and propeller disk area (A_D) of 49.087×10^{-3}.

Table 1. Simulation cases involving various inflow velocities at a fixed rotation speed.

Inflow velocity (V) [m/s]	Advance speed ratio (J) [-]	Rotation speed (n) [rev/s]
1.97	0.53	15
2.11	0.56	15
2.28	0.61	15
2.45	0.65	15
2.59	0.69	15
2.76	0.74	15
2.91	0.78	15
3.07	0.82	15
3.22	0.86	15
3.38	0.90	15
3.54	0.94	15
3.69	0.98	15
3.85	1.03	15
4.00	1.07	15
4.16	1.11	15
4.32	1.15	15
4.46	1.19	15

comparable to the CFD prediction that was obtained in an infinite flow field. Figure 2 shows the boundary conditions applied are: no-slip walls on the propeller and mounting strut; velocity inlet with a specified inflow velocity on the inlet; and opening boundary condition with zero Pa relative pressure at the top, side and bottom boundaries. The cylindrical grid embedding the propeller was connected to the surrounding grid through General Grid Interface (GGI) (ANSYS 2012). The single-phase fluid was prescribed as fresh water, incompressible, and isothermic. Note that the simulation conditions are limited to non-cavitating flow and deep submersion.

4. Results and discussion

4.1. Grid dependence study

A grid dependence study was carried out to ensure the simulation results were consistent and independent of the grid density. Figure 3 shows the grid on $y = 0$ plane where an unstructured tet-grid was adopted with tet-prisms inflation layers to resolve the boundary layer on the surface of the propeller. Note that the investigation kept a calculated y^+ of 12.5 (see details on Section 4.2).

Figure 4 shows the percentage difference of Kt and Kq for each grid level compared to those for the finest grid level (i.e. 14.5 million cells). The propeller rotation speed was set at 15rev/s with an inflow velocity at 4.46 m/s, which is the maximum speed set in the test case (see section 3.2). The results show that further grid refinement beyond approximately 9.3 million grid affects the Kt and Kq by less than 0.6% and 0.4%. However, the required computation time was significantly increased by around 4 times. Given the computational efficiency as well as the acceptable accuracy, the present study selected the 9.3 million grid.

4.2. Influence of near wall gridding with RANS omega-based turbulence model selection

The influence of near wall gridding treatment was evaluated with using omega based RANS turbulence models; the Baseline Reynolds Stress Model (BSLRSM), standard k-omega (k-ω), Shear Stress Transport (SST), omega-based Reynolds Stress Model (Omega RSM), and the Scale-Adaptive Simulation SST (SASSST). The near wall grid was set by a y^+ value representing the first inflation layer height from the surface. Note that the y^+ is defined as the dimensionless distance measured from the propeller blade surface to the first prism layer. The first node wall distance (∂y) reflected by the y^+ value was estimated using $C_{0.7R} \times y^+ \sqrt{80} \times Re_{C_{0.7R}}{}^{(13/14)}$, where $C_{0.7R}$ (i.e. 0.697×10^{-1}) is the maximum span length of the propeller at 0.7 times radius from the centre (White 2003).

In ANSYS CFX, the omega based RANS models utilise the Automatic Wall Treatment (AWT) model for boundary layer modelling. The AWT dictates if the simulation uses the low-Reynolds wall treatment or the wall function formulation for

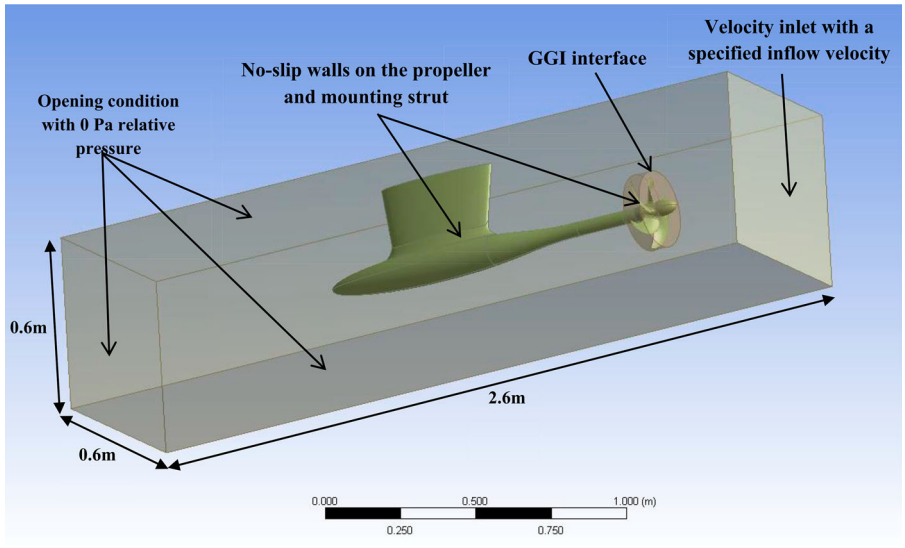

Figure 2. Boundary conditions and arrangement of the propeller in the numerical tank which was replicated by the experimental basin at the Australian Maritime College Cavitation Tunnel (AMCCT).

Note that the blockage correction was made in the experimental data to avoid the interference due to the confinement of the test section walls.

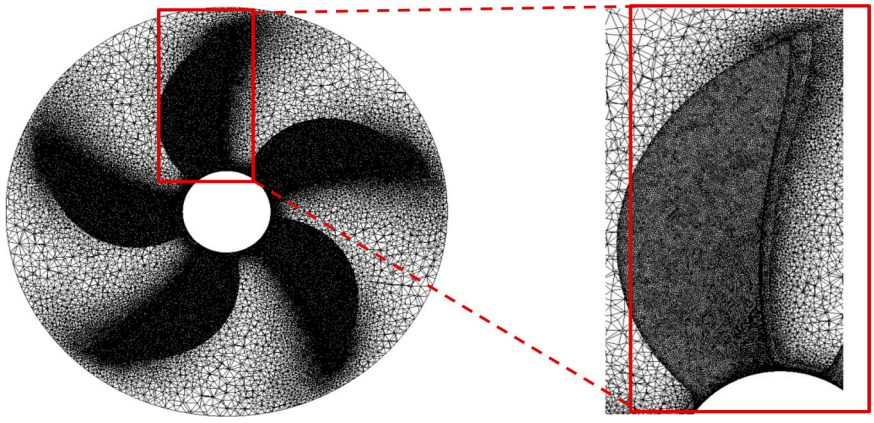

Figure 3. Grid on $y = 0$ plane with a magnified view near a propeller bade.

the boundary layer depending on the first layer y^+. (ANSYS 2012). The current study focuses on using the wall function to reduce computational cost and allow higher grid resolution efforts on the surface of the blades. The AWT in ANSYS CFX effectively switches to the wall function formulation at y^+ values of 11.06 and above (Hally 2009). It is also important that the first layer y^+ does not exceed the log-law region of the boundary layer Thus, the simulations in this study were performed with y^+ values ranging from 12.5 to 120.

Figure 5 shows the *Kt* and *Kq* predictions of the different turbulence models at various y^+ values and the EFD measurements with an error bar indicating the experimental errors (i.e. $Kt = 4.2\%$ and $Kq = 10.2\%$). The simulations were conducted with the maximum inlet speed from the experiment, i.e. 4.46 m/s, and a propeller rotation speed of 15rev/s.

At $y^+ = 12.5$, the *Kt* was under-predicted compared to the experimental measurements. This is like due to the first layer height being too far into the buffer region of the boundary layer for the wall function to be valid. At $y^+ = 25$, the first wall-adjacent node deemed placing in the log law layer, resulting in the minimum descripancy of *Kt* and *Kq* over the various turbulence models. However, at $y^+ = 50$, 75 and 120, the errors of *Kt* and *Kq* become larger due to insufficient resolution in the log law layer. This shows that the lower y^+ enables the better resolution in the log layer region, thus providing the better predictions in *Kt* and *Kq*.

Overall, although SST, SASSST and K-omega provided stable prediction of *Kt* and *Kq* than reynolds stress models (i.e. Omega-RSM and BSLRSM) throughout the y^+ ranges, the reynolds stress models perform better at lower y^+ values (e.g. 12.5 and 25) where the better resolution of log layer was achieved. Further, the BSLRSM with $y^+ = 25$ provided the most accurate predictions in comparison with the EFD measurements (provided by the current EFD testing), thus the combination of BSLRSM and $y^+ = 25$ was adopted for the remainder of this study.

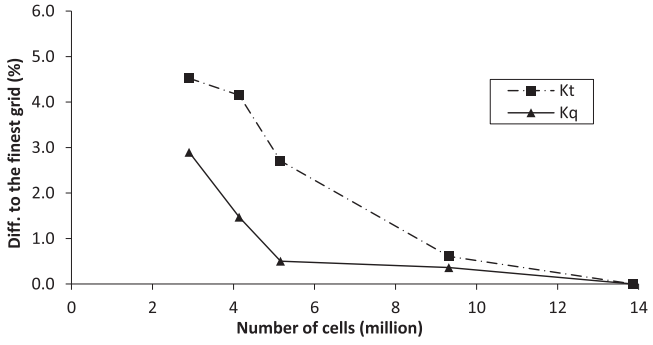

Figure 4. Grid dependence study at a rotation speed of 15rev/s and inflow velocity of 4.46 m/s. A grid at 9.3 million cells was selected in the present study.

4.3. Influence of inflation layer thickness

Various total inflation layer thicknesses were applied to ensure that the boundary layer is sufficiently enclosed within the prescribed inflation layers. A number of thicknesses were estimated based on the experimental based typical boundary layer thickness (i.e. $20 \times 10^{-3} \times C_{0.7R}$) by Carlton (2012), and theoretical estimation by Prandtl (1935) for turbulent flow on a plate, $(0.16 \times C_{0.7R}) / Re_{C_{0.7R}}{}^{1/7}$. As Prandtl`s estimation is for a flat plate, seven different thicknesses (see Table 2) were examined to investigate the sufficient thickness to capture the boundary layer around the curved geometry of the propeller. The investigation was conducted using the BSLRSM turbulence model and a y^+ value of 25. Note that the propeller rotation speed was set at 15rev/s with an inflow velocity at 4.46 m/s.

Figure 6 shows the prediction of the *Kt* and *Kq* as a function of the total inflation layer thicknesses on the blade surface. Both the predicted *Kt* and *Kq* values were found to be independent of the total inflation layer thickness when the thickness value was 1.764×10^{-3} m ($1 \times$ Prandtl's estimate) and above. The predictions from values smaller than this thickness (i.e. Carlton, and 0.25 and 0.5 of Prandtl's estimate) was found to decrease and is attributed to the boundary layer exceed the total inflation layer thickness. As a conservative measure, a total thickness of the inflation layers corresponding to two times Prandtl's estimate was used for the remainder of the study.

4.4. Steady-state vs Transient simulations

The method of propeller rotation was examined to minimise the influence of state conditions (i.e. steady-state and transient) on the prediction. The steady-state based simulation adopted a

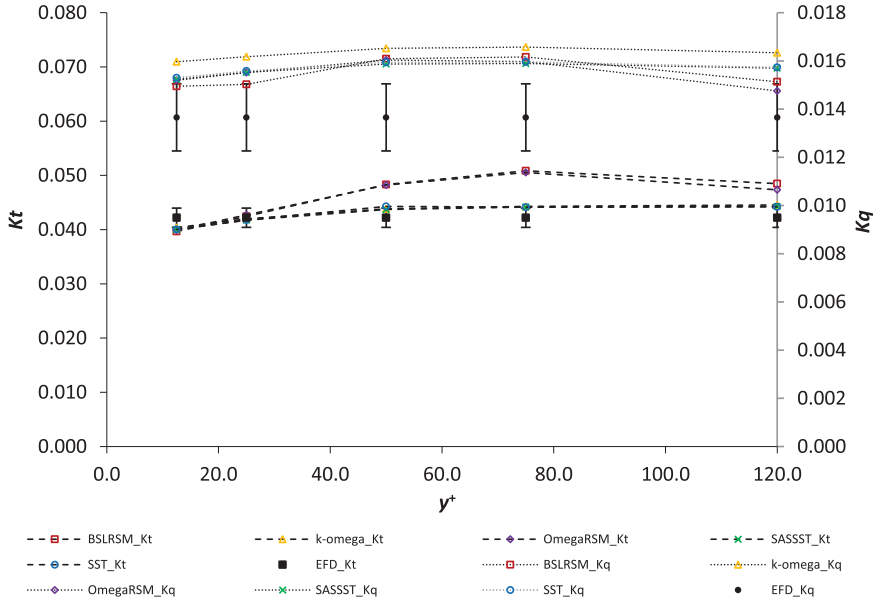

Figure 5. Comparison of the *Kt* and *Kq* between EFD data and CFD prediction using a number of turbulence models at various y^+ values (at 15rev/s and 4.46 m/s inflow velocity), and the EFD measurements with an error bar indicating the experimental errors (i.e. *Kt* = 4.2% and *Kq* = 10.2%).

Table 2. Kt and Kq predictions adopting various total inflation layer thicknesses (at 15rev/s and 4.46 m/s inlet velocity).

Property	Total inflation layer thickness [m]
Carlton (2012)	1.40×10^{-3}
0.25 × Prandtl's estimate	4.411×10^{-4}
0.50 × Prandtl's estimate	8.821×10^{-4}
1 × Prandtl's estimate	1.764×10^{-3}
2 × Prandtl's estimate	3.529×10^{-3}
3 × Prandtl's estimate	5.293×10^{-3}
4 × Prandtl's estimate	7.057×10^{-3}
5 × Prandtl's estimate	8.821×10^{-3}

Table 3. Percentage difference of the Kt and Kq predicted in the transient compared to those in the steady-state condition for the propeller operating at an inlet flow velocity of 4.46 m/s and rotation rate of 15rev/s.

Timestep [s]	Rotation per timestep [degrees/timestep]	Difference (%) to the steady-state condition *Kt*	*Kq*
0.005	27	2.66	3.84
0.001	5.4	2.08	2.91
0.0005	2.7	0.85	1.90
0.0002	1.1	0.79	1.33

frozen rotor method, which utilises a Moving Reference Frame (MRF) to change reference frame with respect to the fixed relative orientation of the components over the interface. On the other hand, the transient based simulation uses a rotor stator method that predicts the true transient interaction of the flow by simulating the transient relative motion between the components on each side of the interfaces. Table 3 shows the percentage difference of *Kt* and *Kq* prediction obtained in transient compared to those in steady-state condition for the propeller operating at an inlet flow velocity of 4.46 m/s and rotation rate of 15rev/s. To minimise the error due to insufficient time discretisation, the transient simulations adopted

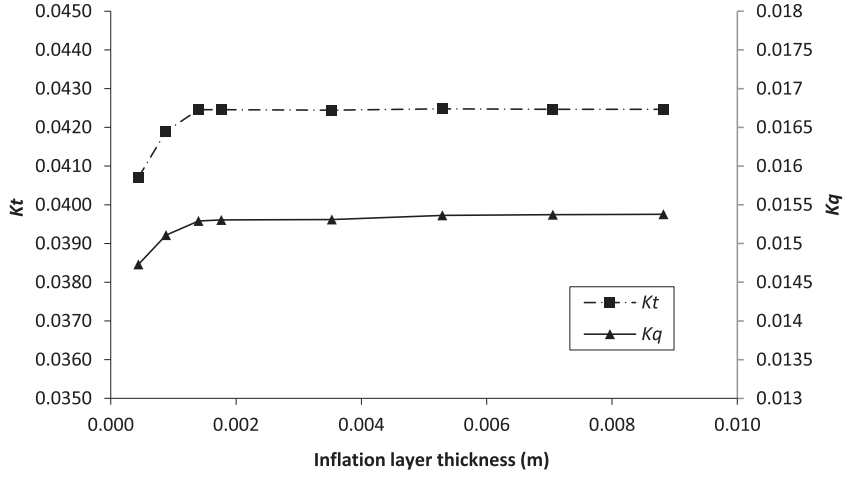

Figure 6. *Kt* and *Kq* predictions over a number of total inflation layer thicknesses calculated based on the experimental based typical boundary layer thickness (i.e. $20 \times 10^{-3} \times C_{0.7R}$) by Carlton (2012), and theoretical estimation by Prandtl (1935) for turbulent flow on a plate.

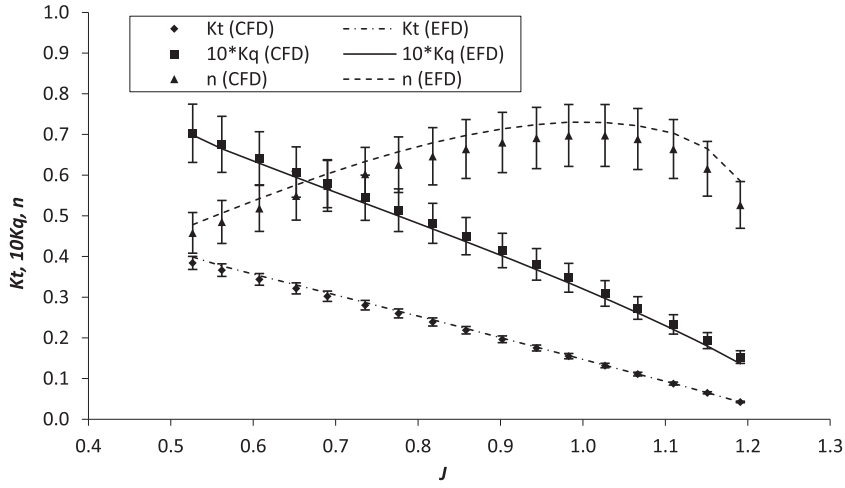

Figure 7. Comparison of the *Kt*, *Kq* and efficiency(η) between CFD predictions and EFD measurements (Norrison et al. 2016) over the advance speed ratio (J) from 0.527 and 1.191, error bars indicate the maximum experimental errors (i.e. $Kt = 4.2\%$, $Kq = 10.2\%$ and $\eta = 10.9\%$).

various time steps ranging from 0.005 s to 0.0002 s corresponding to a propeller rotation of 27–1.1 degrees per each timestep. The results showed the transient simulations with a time step less than 0.0005s predicted the *Kt* and *Kq* within 2% difference compared to those obtained under the steady-state. This indicated with an appropriate time step scale the influence of the state condition on the prediction can be negligible for an openwater propeller. As the steady-state based simulations reduce the computational loads, the remainder of the simulations was performed in steady-state for computational efficiency.

4.5. CFD predictions vs experimental measurements

The prediction of thrust and torque was validated against experimental data for various inflow velocities ranging from 1.97 m/s to 4.47 m/s at 15rev/s. Figure 7 shows *Kt*, *Kq* and efficiency (η) as a function of *J*. The prediction of *Kt* was in very good agreement with the EFD data (Norrison et al. 2016) within 3.5%. However, *Kq* was overpredicted by a maximum of 10.2% at the highest *J*. This is attributed to that the CFD predictions were obtained under the fully turbulent flow regime. As stated in Carlton (2012) and Rhee and Joshi (2005) the model scale experiment can cause a laminar region existing on the blade suction side, resulting in less torque generation in the experiment. As the torque was over-predicted, the laminar region on the propeller blade was considered the main source of the discrepancy. Another cause of the discrepancy is sensitivity limit of the measurement in the experiment whereby the torque become increasingly difficult to measure as it is relatively small at higher *J*.

5. Conclusions

This paper presented a systematic investigation over the methodology of RANS based numerical computation to predict the hydrodynamic characteristics of a propeller operating in a uniform fluid flow. The investigation included detailed methodology of RANS-based simulation containing the turbulence model selection among the omega-based turbulence models with the required grid conditions (i.e. first grid layer height, y^+ and total inflation layer thickness), also including the appropriate simulation settings (i.e. steady-state and transient conditions, and time step). In order to reduce computational load associated with the grid resolution, the wall formulation was used in modelling boundary layer for the simulations.

Five omega based turbulence models were investigated in this study: the Baseline Reynolds Stress Model (BSLRSM), standard k-omega (k-ω), the Shear Stress Transport (SST), the Omega-based Reynolds Stress Model (Omega RSM) and the Scale-Adaptive Simulation SST (SASSST). It was found that the BSLRSM predictions at $y^+ = 25$ provided the most promising results with good agreement against the experimental measurements. Investigation of the effect of total inflation layer thickness on the numerical predictions recommends that the minimum thickness to be at least be equal to Prandtl's 1/7th power law estimate of a turbulent boundary layer thickness over the maximum span length of the propeller at 0.7 times radius from the centre. Under-prescribing the total thickness resulted in lower *Kt* and *Kq* predictions compared to the recommended thickness, while over-prescribing the total thickness showed no perceptible differences in prediction. In addition, it was confirmed that the influence of the state condition (i.e. steady-state and transient conditions) can be negligible with an appropriate timestep scale in the transient for an openwater propeller.

From the comparison with the experimental data, the CFD results showed a good agreement against experirmental data within 3.5% for *Kt* and 10.2% for *Kq*. The overprediction of *Kq* is attributed to the laminar region existing on the propeller blade surface, thus suggesting further work to resolve the laminar region in the computations. Overall, the validity of the present CFD methodology was proven for the prediction of the propulsion properties. The proposed methodology will be applied to the upcoming work on free running submarine simulations based on the work reported by Kim et al. (2018). This current study can be extended to assess and validate the effect of a non-uniform fluid flow (e.g. oblique flow) and the presence of the hull on the propeller performance.

Acknowledgement

The authors wish to thank Paul Brandner and Bryce Pearce of the Australian Maritime College Cavitation Research Laboratory and the Defence Science and Technology Group for providing experimental data for comparison with the CFD.

Disclosure statement

No potential conflict of interest was reported by the authors.

ORCID

Howan Kim http://orcid.org/0000-0003-2992-9115
Zhi Quan Leong http://orcid.org/0000-0002-0644-1822

References

ANSYS. 2012. ANSYS CFX-solver theory guide. ANSYS Release. 14(5): 86–96.

Carlton J. 2012. Marine propellers and propulsion. Butterworth-Heinemann.

Guilmineau E, Deng GB, Leroyer A, Queutey P, Visonneau M, Wackers J. 2014. Wake simulation of a marine propeller. Paper presented at the 11th World Congress on computational mechanics; Barcelona.

Hally D. 2009. Grid dependence of RANS codes for flows past propeller blade sections.

Kim H. 2018. Six-DOF motion response and manoeuvring simulation of an underwater vehicle [PhD]. University of Tasmania.

Kim H, Leong Z, Ranmuthugala D, Clarke D, Binns J, Duffy J. 2018. Numerical investigation into the effect of incidence flow angles on submarine propeller hydrodynamic characteristics.

Kim H, Ranmuthugala D, Leong Z, Chin C. 2018. Six-DOF simulations of an underwater vehicle undergoing straight line and steady turning manoeuvres. Ocean Eng. 150:102–112.

Lu NX, Svennberg U, Bark G, Bensow R. 2012. Numerical simulations of the cavitating flow on a marine propeller. Paper presented at the 8th International Symposium on Cavitation.

Morgut M, Nobile E. 2012. Influence of grid type and turbulence model on the numerical prediction of the flow around marine propellers working in uniform inflow. Ocean Eng. 42:26–34.

Norrison D, Anderson B SW, Petterson K, Fureby C. 2016. Numerical study of a self-propelled conventional submarine. Paper presented at the 31st Symposium on Naval Hydrodynamics; Monterey, California.

Peng HH, Qiu W, Ni S. 2013. Effect of turbulence models on RANS computation of propeller vortex flow. Ocean Eng. 72:304–317.

Prandtl L. 1935. The mechanics of viscous fluids.

Rhee SH, Joshi S. 2005. Computational validation for flow around a marine propeller using unstructured mesh based Navier-Stokes solver. JSME Int J Ser B Fluids Therm Eng. 48(3):562–570.

Wang C, Sun S, Sun S, Li L. 2017. Numerical analysis of propeller exciting force in oblique flow. J Mar Sci Technol. 22(4):602–619.

White FM. 2003. Fluid mechanics. New York: McGraw-Hill.

Yao J. 2015. Investigation on hydrodynamic performance of a marine propeller in oblique flow by RANS computations. Int J Naval Archit Ocean Eng. 7(1):56–69.